Shyu *et al.*
Progress in Earth and Planetary Science (2024) 11:41
https://doi.org/10.1186/s40645-024-00644-9

Progress in Earth and Planetary Science

RESEARCH ARTICLE Open Access

Assessing the relative activity of faulting along both flanks of the Ou Backbone Range, Tohoku Region, Japan, from fluvial geomorphic analyses

J. Bruce H. Shyu[1*], Jhih-Hao Liao[1], Chia-Yu Chen[1,2], Hiroyuki Tsutsumi[3] and Yasufumi Iryu[4,5]

Abstract

The Ou Backbone Range in the Tohoku Region of Japan is bounded on its both sides by two major active fault systems: the Western Fault Zone of Kitakami Lowland in the east and the Eastern Fault Zone of Yokote Basin in the west. Although these two systems are primary active fault systems in the region, information on their long-term activity characteristics is still quite limited. Therefore, we analyzed the normalized channel steepness indexes of river valleys trending perpendicular to the range front along both flanks of the Ou Backbone Range. Our results show that the eastern flank has gentler river valleys, whereas rivers along the northwestern flank are steeper. Our field investigation shows that knickpoints in this area are mostly related to local lithologic boundaries or are check dams along the valleys, thus the river systems are likely under steady-state conditions. Hence, the steeper river valleys in northwestern Ou Backbone Range indicate a higher uplift rate of the area. Because both fault systems are primarily dip-slip reverse faults and do not have significant variations in their subsurface geometry, the faster uplift suggests that the northern segment of the Eastern Fault Zone of Yokote Basin has a higher slip rate. This is consistent with results of previous studies, and the fact that the rupture of the 1896 Rikuu earthquake, the only historical surface-rupturing event in this region, was only limited along the northern segment of this fault system.

Keywords Active faults, Normalized river steepness index, Ou Backbone Range, Tohoku Region, Japan

1 Introduction

The Ou Backbone Range (OBR) is one of the most prominent geomorphic features in the Tohoku (northeastern) Region of Japan, which is located within one of the most seismically active plate boundary belts in the world (Headquarters for Earthquake Research Promotion 2009; Fig. 1). Bordering the OBR on both sides are the Yokote Basin and the Kitakami Lowland, both of which have a long history of agriculture development and settlement establishment. The mountain fronts between the range and the basin/lowland on its both sides are characterized by two active fault systems, the Eastern Fault Zone of Yokote Basin (EFZYB) along the western front of the range and the Western Fault Zone of Kitakami Lowland (WFZKL) along the eastern front of the range

*Correspondence:
J. Bruce H. Shyu
jbhs@ntu.edu.tw
[1] Department of Geosciences, National Taiwan University, Taipei, Taiwan
[2] Department of Earth and Environmental Sciences, National Chung Cheng University, Chiayi, Taiwan
[3] Department of Environmental Systems Science, Faculty of Science and Engineering, Doshisha University, Kyotanabe, Japan
[4] Institute of Geology and Paleontology, Graduate School of Science, Tohoku University, Sendai, Japan
[5] Advanced Institute for Marine Ecosystem Change (WPI-AIMEC), Tohoku University, Sendai, Japan

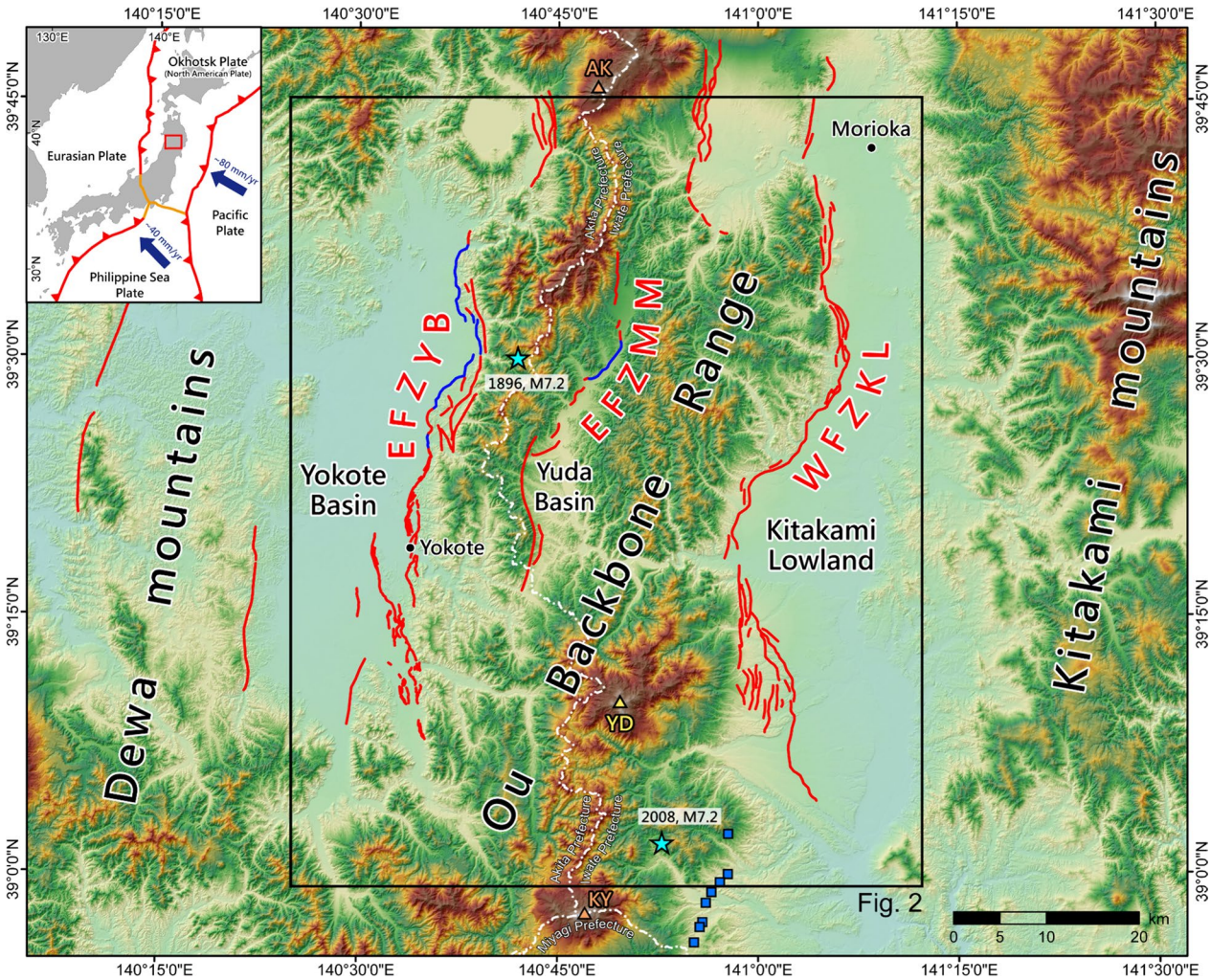

Fig. 1 Map showing the study area. The Ou Backbone Range (OBR) is one of the most prominent geomorphic features in the Tohoku Region of Japan. The mountain range is bounded on its both sides by the Eastern Fault Zone of Yokote Basin (EFZYB) along the western front of the range and the Western Fault Zone of Kitakami Lowland (WFZKL) along the eastern front of the range. In the central part of the northern OBR, the Eastern Fault Zone of Mahiru Mountains (EFZMM) on the western side of the intermontane Yuda Basin is generally considered as a backthrust that branches out from the EFZYB (e.g., Kagohara et al. 2009; Arora et al. 2021). The 1896 M7.2 Rikuu earthquake was produced by ruptures of the northern segment of the EFZYB, with some surface ruptures observed along a segment of the EFZMM. Fault traces are from Research Group for Active Faults of Japan (1991), Nakata and Imaizumi (2002), and Headquarters for Earthquake Research Promotion (2001, 2005a, b). Location of the 1896 epicenter and the surface ruptures during the earthquake (shown in blue) are from Matsuda et al. (1980). Location of the 2008 epicenter is from Matsu'ura and Kase (2010), and the 2008 surface rupture locations (shown as blue squares) are from Toda et al. (2010). Orange triangles indicate two active volcanoes in this region (AK: Akita Komagatake; KY: Kurikoma Yama), and the yellow triangle indicates the Yakeishi Dake (YD), a prominent Quaternary volcano. Volcano data are from Nakano et al. (2013) and Geological Survey of Japan, AIST (2020)

(e.g., Research Group for Active Faults of Japan 1991; Nakata and Imaizumi 2002; Headquarters for Earthquake Research Promotion 2001, 2005a). The EFZYB is an east-dipping reverse fault, and the WFZKL is a reverse fault that dips to the west (Headquarters for Earthquake Research Promotion 2001, 2005a; Sato et al. 2002). These two fault systems likely converge at a depth of ~ 13 km, making a pop-up structure that forms the OBR (e.g., Sato et al. 2002).

Both of these two fault zones are considered and evaluated among the 115 major active faults by the Headquarters for Earthquake Research Promotion (HERP) of Japan (https://www.jishin.go.jp/evaluation/long_term_evaluation/major_active_fault/). These faults pose significant seismic hazard for the settlements of the basin/lowland, as demonstrated by the 1896 M7.2 Rikuu earthquake, which was produced by ruptures of the northern segment of the EFZYB and was one of the largest on-land reverse

faulting earthquakes in the history of Japan (e.g., Matsuda et al. 1980; Figs. 1 and 2).

There have been many previous studies to understand the long-term (10^3 to 10^5 years) activity of the two major fault systems, including paleoseismological studies on various sites along the faults and geomorphic analyses of fluvial terraces along rivers flowing out of the range to quantify the incision/uplift rate of the range (e.g., Matsuda et al. 1980; Research Group for the Senya Fault 1986; Imaizumi et al. 1997, 1989a, b; Tajikara and Ikeda 2005; Kagohara et al. 2009; AIST 2010). However, being the seismogenic structure of the 1896 Rikuu earthquake, most of the efforts have been focused on the northern segment of the EFZYB. Information on the long-term characteristics of other segments of these two fault systems is still quite limited. Furthermore, many of the

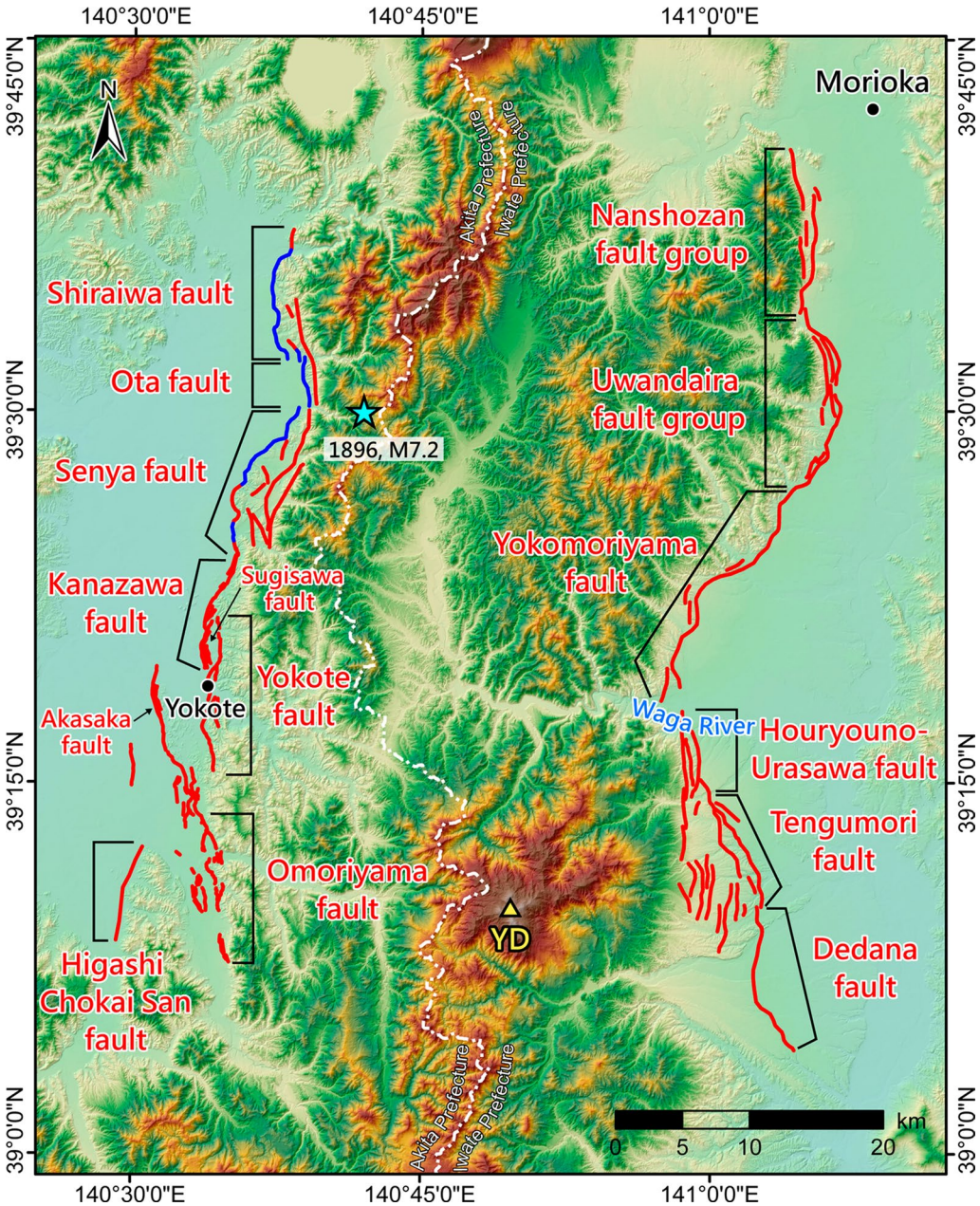

Fig. 2 Detailed fault segments of the EFZYB system and the WFZKL system. Fault names are adapted from Research Group for Active Faults of Japan (1991), Nakata and Imaizumi (2002), AIST (2010), and Sawa et al. (2013). Surface ruptures during the 1896 Rikuu earthquake (shown in blue) are from Matsuda et al. (1980). YD: Yakeishi Dake

data were obtained from isolated trenching sites along the faults, or from one of the fault branches that may not be representative for the entire fault system. As a result, different ideas exist for the 10^3-to-10^5-year activity characteristics of these faults. For example, whereas many previous studies suggest that the slip rates along the southern segment of EFZYB is lower than that along the northern segment (e.g., Headquarters for Earthquake Research Promotion 2005a), a recent study along a branch fault of its southern segment indicate that the slip rates along the entire EFZYB may be similar (Arora et al. 2021).

For the past two decades, fluvial geomorphic indices have been widely applied to study active deformations in orogenic belts (e.g., Kirby and Whipple 2012). This is based on the assumption that rivers, as the connection between the uplifting mountain belts and the base level, are the first-order control of the landscape relief and to transmit the tectonic forcing signals of the orogen. One of the most frequently used indices is the channel steepness index of river valleys that flow out of mountain belts, which has been shown to provide information about the general long-term uplift patterns of the mountain belt (e.g., Kirby and Whipple 2012; Chen et al. 2015). Since the channel steepness index generally reflects the conditions of the entire drainage basin, it would also provide information with a wider spatial extent than that obtained near the fault trace. Patterns of fluvial channel steepness indexes have been applied to understand characteristics of active faults (e.g., Kirby and Ouimet 2011; Harvey et al. 2015), uplift patterns along mountain belts (e.g., Kirby and Whipple 2012; Miller et al. 2013; Chen et al. 2015), and the relationship between tectonic uplift and erosional processes across various mountain belts (e.g., Harkins et al. 2007; Cyr et al. 2010; DiBiase et al. 2010; Chen et al. 2021; DeLisle et al. 2022).

Despite the fact that this method has been applied to many orogenic belts in the world, it has only been applied scarcely in Japan (e.g., Regalla et al. 2013; Ogami 2015; Takahashi et al. 2022, 2023). Therefore, this study aims to understand the long-term activity characteristics of both the EFZYB and the WFZKL based on the analysis of channel steepness indexes of river valleys flowing out of the OBR to delineate the variation of uplift rates of the hanging-wall block along these fault systems. We have also compared our results with data from previous studies.

Our study provides one of the few results of geomorphic indexes applied to understanding the uplift of mountain ranges in Japan. Not only are these results important in assessing future earthquake hazard in the Tohoku Region of Japan, but they also demonstrate the applicability of fluvial geomorphic analysis in providing additional constraints for understanding active faults in other parts of this important orogenic belt.

2 Geological background of the Ou Backbone Range

The OBR is one of the most prominent topographic features in northern Japan, spanning ~ 100 km and forms the boundary between the Iwate and Akita Prefectures (Fig. 1). On the western side of the range is the Yokote Basin that separates the OBR and the Dewa Mountains further to the west. On the eastern side of the range is the Kitakami Lowland, which is also a young fluvial basin that separates the OBR and the Kitakami Mountains in the east.

Rocks within the OBR generally consist of Miocene andesitic lava and pyroclastic rocks that are overlain by Miocene to Pleistocene marine to terrestrial sedimentary rocks (e.g., Kagohara et al. 2009; Geological Survey of Japan, AIST 2023; Fig. 3). Quaternary volcanoes are present mostly in the eastern part of the range, with the Yakeishi Dake having the most prominent landform. The most recent activity of this Pleistocene volcano is at ca. 0.2 Ma, and its surrounding area is composed of lava flow and pyroclastic flow deposits from the volcano (Nakano et al. 2013; Geological Survey of Japan, AIST 2020, 2023). Two active volcanoes (Akita Komagatake, AK, and Kurikoma Yama, KY) are present at the northern and southern end of the OBR (Nakano et al. 2013; Geological Survey of Japan, AIST 2020; Fig. 1).

Along both sides of the OBR are two major active fault systems identified and listed by the Headquarters for Earthquake Research Promotion (HERP) of Japan. Between the OBR and the Yokote Basin in the west, the EFZYB is composed of the Shiraiwa fault, the Ota fault, the Senya fault, the Kanazawa fault, the Yokote fault, and the Omoriyama fault from north to south (e.g., Research Group for Active Faults of Japan 1991; Nakata and Imaizumi 2002; AIST 2010; Fig. 2). Some previous studies have also mapped the Sugisawa fault to the east of the Kanazawa fault north of Yokote (e.g., Sawa et al. 2013). West of the Yokote fault, the northern extension of the Omoriyama fault along the western edge of a series of low-lying hills has also been named as the Akasaka fault (e.g., Sawa et al. 2013). South of the Akasaka fault, the Higashi Chokai San fault along the western edge of the Yuzawa Hills is sometimes considered as a frontal branch of the EFZYB system (e.g., Research Group for Active Faults of Japan 1991; Sawa et al. 2013). In the east between the OBR and the Kitakami Lowland, the WFZKL consists of the Nanshozan fault group, the Uwandaira fault group, the Yokomoriyama fault, the Houryouno-Urasawa fault, the Tengumori fault, and the Dedana fault from north to south

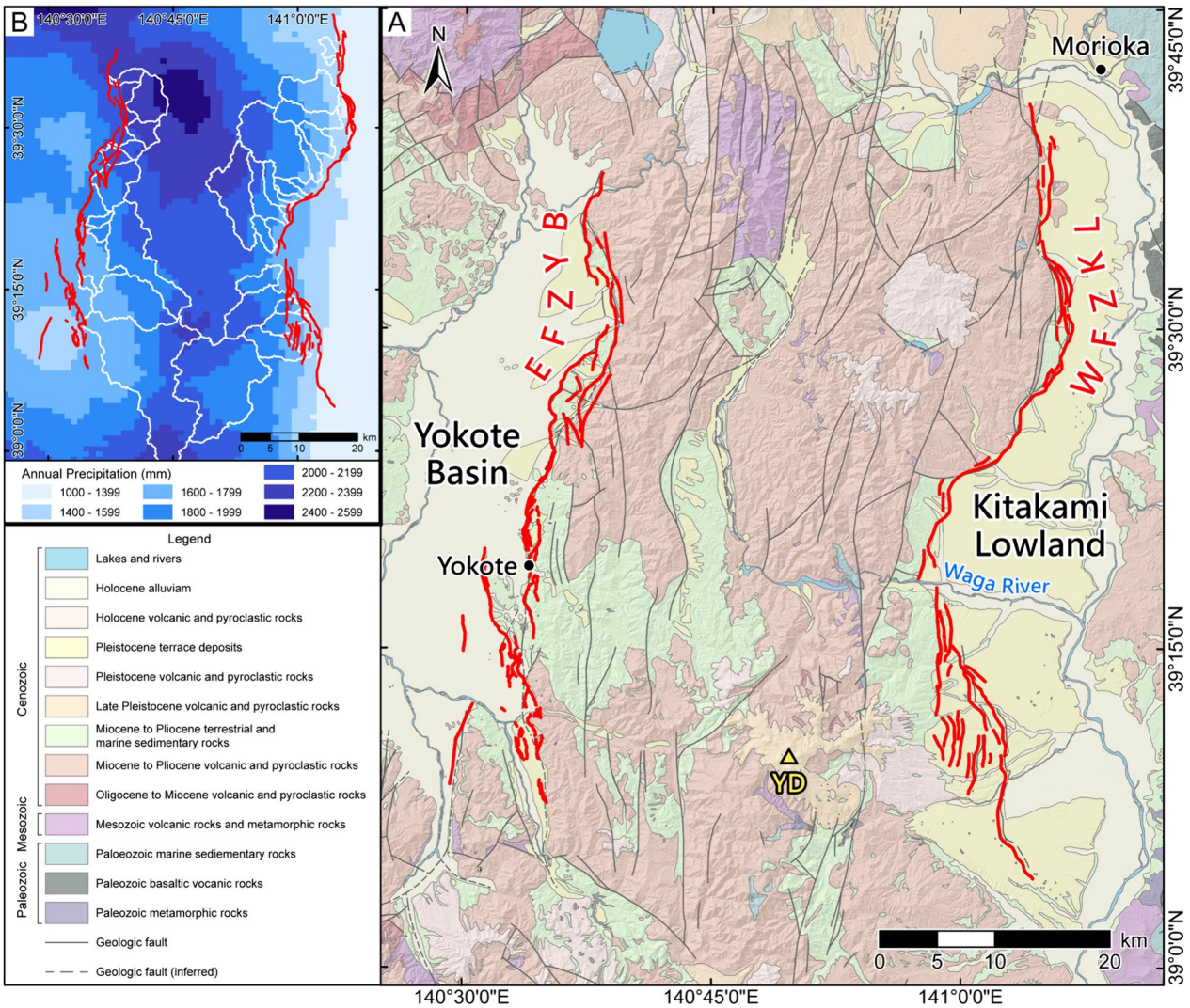

Fig. 3 **A** Simplified geologic map of the OBR region. Data from https://gbank.gsj.jp/seamless/v2/viewer/ (Geological Survey of Japan, AIST 2023). YD: Yakeishi Dake. **B** Annual precipitation patterns of the study area. Data from https://nlftp.mlit.go.jp/ksj/gml/datalist/KsjTmplt-G02.html

(Research Group for Active Fault of Japan 1991; Nakata and Imaizumi 2002; Fig. 2).

Both the EFZYB and the WFZKL are considered as primarily dip-slip reverse fault, and no strike-slip component has been identified or reported (Headquarters for Earthquake Research Promotion 2001, 2005a). Based on seismic reflection survey data, the northern segment of the EFZYB dips eastward at 20°–35° at depths shallower than ~ 1.5 km, and becomes ~ 45° at deeper depths (Sato et al. 2006; Kagohara et al. 2009). Data for the southern segments of the EFZYB is limited, but the fault appears to dip at about 45° to the east (AIST 2010). However, Arora et al. (2021) found that the shallow part of the Omoriyama and Higashi Chokai San faults may have similar gentle dip (20°–30°) as the northern EFZYB. The WFZKL has a similar fault geometry as the EFZYB. Near surface, the fault dips westward at 20°–30°, and becomes 30°–40° to a depth of 7–8 km (Headquarters for Earthquake Research Promotion 2001; Kagohara et al. 2011).

The northern segment of the EFZYB, including the Shiraiwa fault, the Ota fault, and the Senya fault, ruptured in 1896 in the M7.2 Rikuu earthquake (e.g., Matsuda et al. 1980; Research Group for the Senya Fault 1986; Fig. 2). In contrast, the other segments of these two fault systems do not have any historical surface-rupturing earthquake record, but the M7.2 (Mw 6.9) Iwate-Miyagi Nairiku earthquake in 2008 was accompanied by discontinuous surface ruptures southwest of the Dedana fault, probably along a previously unmapped fault in the hanging-wall

block of WFZKL's southern extension (e.g., Matsu'ura and Kase 2010; Toda et al. 2010; Fig. 1).

There are many previous studies on the Holocene earthquake history and the slip rates of these two fault systems. Along the northern EFZYB, for example, paleoseismological studies along the 1896 rupture revealed that the penultimate event prior to 1896 occurred at ca. 3.5 ka, thus the earthquake recurrence interval for the northern EFZYB is proposed to be around 3400 years (Research Group for the Senya Fault 1986; Imaizumi et al. 1989a, 1989b; Headquarters for Earthquake Research Promotion 2005a). Along the southern EFZYB, the most recent earthquake event was found to be after ca. 6–5 ka, but the fault was not activated in 1896 (Akita Prefecture 1998a, b, 1999). Along the WFZKL, on the other hand, paleoseismological studies found that the most recent earthquake event was ca. 4.5 ka, with a penultimate event sometime between 30 and 7 ka (Watanabe et al. 1994; Iwate Prefecture 1996).

Late Pleistocene or Holocene fault slip rates or vertical separation rates of the two fault systems have been determined mainly using the deformation amount of terraces across the faults and their ages. For example, an average late Holocene slip rate of the northern EFZYB was estimated at about 0.8 mm/yr (Matsuda et al. 1980). Late Pleistocene dip-slip rate of this segment has been calculated at about 0.9–1.2 ± 0.3 mm/yr (Imaizumi et al. 1997; Kagohara et al. 2009; Matsu'ura and Sugaya 2017), slightly higher than the late Holocene rate. Along the southern EFZYB, data on the slip rates are fewer, but it is generally considered that the faults slip slower than the northern segments, at about 0.2–0.3 mm/yr (Akita Prefecture 1998a, b; AIST 2010). However, Arora et al. (2021) recently reported a slip rate of 1.6–1.9 mm/yr over the past 3.5 ka of the Higashi Chokai San fault, based on borehole studies across the fault. This rate appears to be similar to, or even greater than that along the northern segment of the EFZYB.

Along the WFZKL, geomorphic analyses have determined that the Late Pleistocene to Holocene slip rate of its northern segment is about 0.2–0.6 mm/yr (Nakata 1976; Iwate Prefecture 1998a, b). Based on the horizontal shortening amount reconstructed from the faulted strata, Kagohara et al. (2011) estimated a vertical separation rate of ~0.4 mm/yr since ca. 700 ka for the northern WFZKL, which would correspond to a slip rate of ~0.6 mm/yr if the fault dips at ~40°. For the southern segment of the WFZKL, Iwate Prefecture (1997) proposed a Late Pleistocene to Holocene slip rate of about 0.2 mm/yr. Further to the south, in the areas of the Dedana fault (the southernmost segment of the WFZKL) and the surface ruptures of the 2008 Iwate-Miyagi Nairiku earthquake, vertical separation rates of ~0.1–0.5 mm/yr across the fault traces have been estimated from fluvial terrace studies (e.g., Watanabe 1989; Matsu'ura et al. 2008; Tajikara et al. 2009; Goto and Sasaki 2019).

In the central part of the northern OBR, an intermontane Yuda Basin is present (Fig. 1). Along the western edge of this basin, there is an Eastern Fault Zone of Mahiru Mountains (EFZMM; Headquarters for Earthquake Research Promotion 2005b), which is generally considered as a backthrust that branches out from the EFZYB at a depth around 10 km (e.g., Kagohara et al. 2009; Arora et al. 2021). In the middle segment of the EFZMM, some surface ruptures were also observed during the 1896 Rikuu earthquake (Matsuda et al. 1980).

3 Methods

Normalized channel steepness (k_{sn}) has been shown to have a positive relationship with erosion rate and hence can be used to obtain a first-order view of the tectonic pattern from the landscape (DiBiase et al. 2010; Kirby and Whipple 2012). In this study, we used a simplified form of the stream power model for erosion rate, which states that erosion rate is a function of rock erodibility (K), upstream area (A), and channel slope (S) (Howard and Kerby 1983; Whipple and Tucker 1999), and considered mass balance that the change of elevation (z) of a channel point through time (t) and space (x) is determined by the differences between uplift rate (U) and erosion rate (Eq. 1):

$$\frac{\partial z(t,x)}{\partial t} = U(t,x) - KA^m\left(\frac{\partial z(t,x)}{\partial x}\right) \tag{1}$$

where m and n are positive constants relating to the mechanical process of erosion, hydraulic geometry, and basin hydrology.

Instead of using the convention way to derive channel steepness with slope-area relation of channels (e.g., Kirby and Whipple 2012), we used the integral approach, χ analysis, to bedrock rivers proposed by Perron and Royden (2012), which uses elevation data directly instead of its derivatives. Assuming uplift rate and rock erodibility are spatially and temporally uniform, the steady-state elevation of a channel point can be calculated from the base level $z(x_b)$ as a function of channel steepness, $\left(\frac{U}{K}\right)^{\frac{1}{n}}$, and χ:

$$z(x) = z(x_b) + \left(\frac{U}{KA_0^m}\right)^{\frac{1}{n}}\chi \tag{2}$$

where:

$$\chi = \int_{x_b}^{x}\left(\frac{A_0}{A(x')}\right)^{\frac{m}{n}}\mathrm{d}x' \tag{3}$$

and A_0 is an arbitrary scaling area to give χ dimensions of length.

We used a 10-m resolution DEM of Japan obtained from the Geospatial Information Authority of Japan. To avoid the analyses of colluvial and alluvial channels where the stream power model may not be valid, we set a critical area of 1 km^2. This critical area is set according to the change of relations between slope and area, which suggests that channels with drainage basin area smaller than this are dominated by debris flows and colluvial processes. We also removed the alluvial area, including footwall regions of both the EFZYB and the WFZKL, and the Yuda Basin in the middle of the OBR, so that the analysis is focusing on the bedrock channels. We used TopoToolbox 2 that was developed by Schwanghart and Scherler (2014), to extract channels and calculate χ values with a m/n value of 0.45 and an A_0 value of 1 km^2. The k_{sn} values were then calculated by dividing the difference in z by the difference in χ for each channel reach with a moving window of 250 m.

We analyzed a total of 31 river basins along the two sides of the OBR (Fig. 4). We primarily chose the drainage basins that flow out of the OBR across either the EFZYB or the WFZKL to compare the river steepness patterns of the hanging-wall blocks of these two fault systems. Since rivers flowing into the Yuda Basin do not flow across the faults, we excluded those river basins in our analysis. On the other hand, the river systems north of our analyzed basins have upstream tributaries flowing out of the Akita Komagatake volcano (AK in Fig. 1), which is an active volcano (Nakano et al. 2013; Geological Survey of Japan, AIST 2020). Therefore, we also excluded those river systems from our analysis. Among the 31 basins, 12 are located along the western OBR and flow into the Yokote basin, and 19 are located along the eastern OBR and flow into the Kitakami Lowland.

In addition to deriving channel steepness for each channel reach, we also calculated basin-wide mean local steepness (MLS) for the 31 basins in our study area in order to characterize the spatial variance of uplift rate along both flanks of the OBR. MLS is calculated following the method proposed by Chen and Willett (2016). Each local channel steepness is weighted by its local upstream area, and the MLS is the mean of the local area-weighted channel steepness of all channel reaches in a basin.

4 Results

4.1 River steepness patterns along both flanks of the Ou Backbone Range

The k_{sn} results of the 31 river basins we analyzed are shown in Fig. 4. Along both flanks of the OBR, the k_{sn} value distribution show a difference between the northern part and southern parts of the range flanks. Along the eastern flank of the OBR, the k_{sn} values are generally higher in basins in the south than those in the north. In Fig. 4, this is illustrated by the generally warmer colors of k_{sn} values that appear along the river segments in the drainage basins in the southern part of the eastern OBR mountain front, south of the Waga River. In contrast, along the western flank of the OBR, the k_{sn} values in basins north of Yokote are generally higher, especially those flowing across the segment of the EFZYB that ruptured in the 1896 Rikuu earthquake (Fig. 4).

4.2 Knickpoints observations of the Ou Backbone Range rivers

In our analysis, we have identified many knickpoints along the 31 river valleys that drain the two sides of the OBR. Since the presence of certain types of knickpoints may indicate that the river valleys are out of topographic steady state (e.g., Kirby and Whipple 2012), we also conducted field investigations to understand the characteristics of the knickpoints.

Our investigation results indicate that almost all of the knickpoints identified in the OBR rivers are related to local lithologic boundaries or are check dams along the valley (Fig. 5; Additional file 1: Fig. S1). We were unable to access a few knickpoints, but most of those are located along upstream segments of the rivers. Therefore, even if those knickpoints that we did not investigate were tectonic knickpoints, they do not significantly affect the general k_{sn} patterns of the river basins. As a result, we conclude that the OBR river basins are generally under topographic steady state.

4.3 Basin-wide mean local steepness of the Ou Backbone Range rivers

To better compare the k_{sn} patterns of river basins along the two sides of the OBR, we further calculated the basin-wide mean local steepness (MLS) of the 31 basins. The MLS values of the 12 river basins along the western OBR front are between ~19 and ~70, and the MLS values of the 19 basins in the east are between ~16 and ~55 (Table 1). The MLS values have similar trends as the k_{sn} values, that is, along the western OBR front, the northern basins north of Yokote have higher MLS values than the southern basins; along the eastern OBR front, the southern basins south of the Waga River have higher MLS values (Fig. 5). Among them, the northwestern OBR river basins have generally the highest values of MLS.

5 Discussion

5.1 Mechanisms affecting steepness indexes of rivers

Nontectonic processes, especially climatic changes and lithological differences, may affect the k_{sn} values of river segments. However, based on the weather information

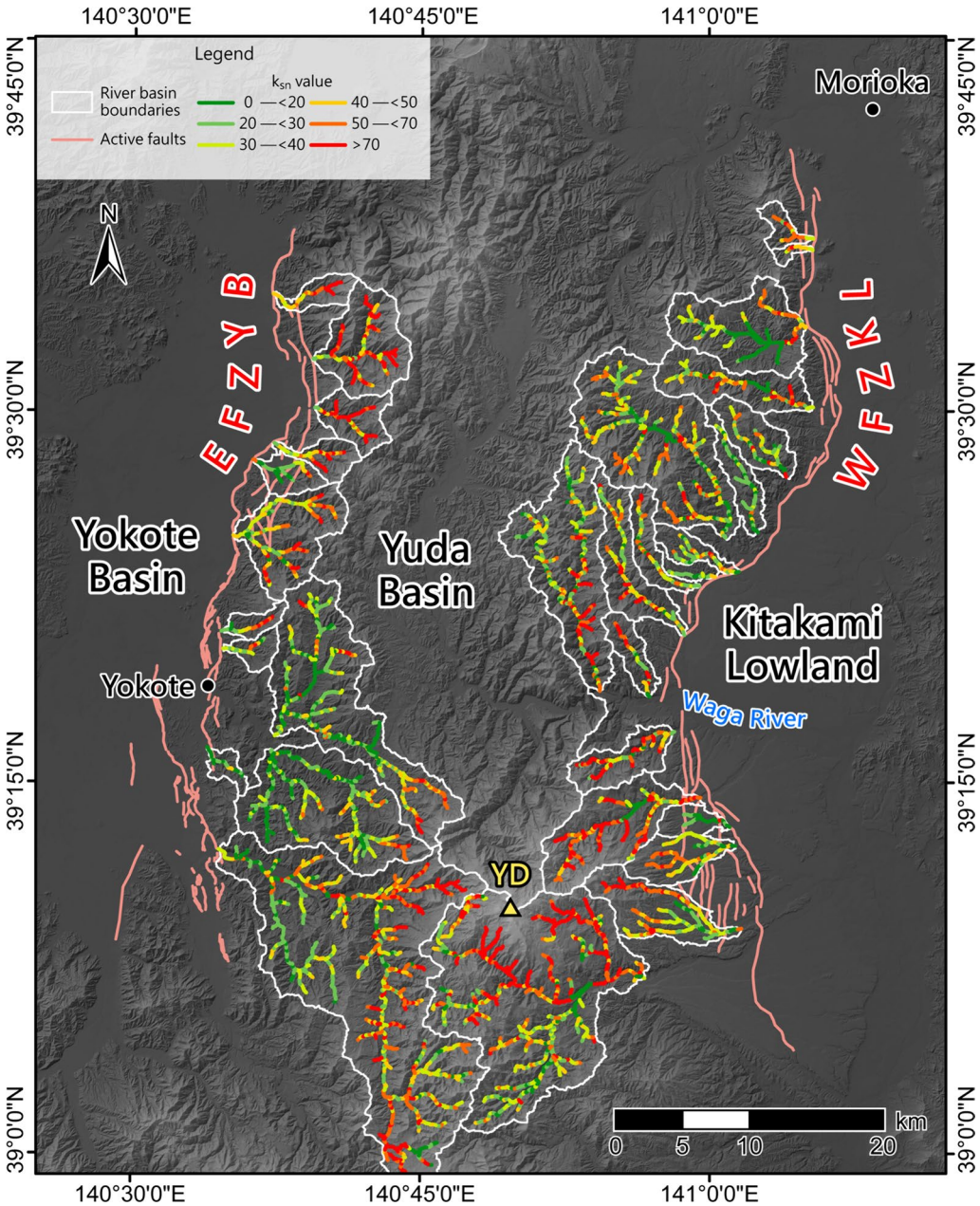

Fig. 4 River steepness index (k_{sn}) of the 31 analyzed river basins on both sides of the OBR. We excluded the rivers flowing into the Yuda Basin since they do not flow across the fault systems. YD: Yakeishi Dake

available from the Japan Meteorological Agency, the river basins we analyzed are all located at regions with similar precipitation (Fig. 3B), and the pattern of precipitation is generally reflecting the changes in elevation from lowland or basins to the drainage divides, without an obvious latitudinal trend. Furthermore, we calculated the mean annual precipitation for each basin and compared it with MLS (Additional file 2: Fig. S2). The result shows that there seems to be a weak positive relationship between these two values. However, based on the stream power model, higher precipitation will result in a higher rock erodibility (K) and lower MLS. This is opposite to their positive relationship, and suggests that the precipitation is not the primary control of the MLS values. Therefore, it is unlikely that the k_{sn} differences among the OBR river basins are primarily produced by differences in climate conditions.

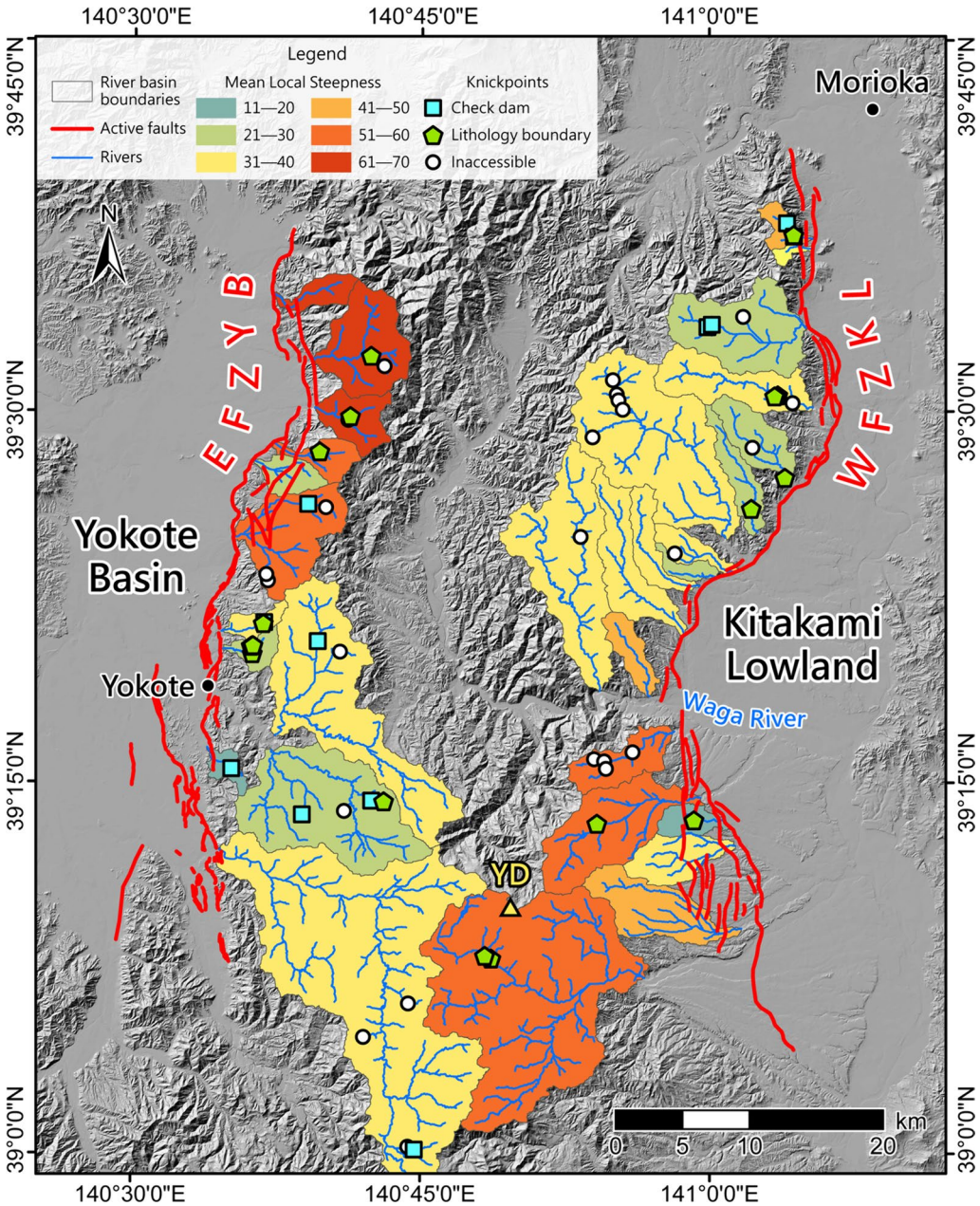

Fig. 5 Basin-wide mean local steepness (MLS) of the 31 basins analyzed in this study. The highest values of MLS are generally found in river basins along the northwestern OBR, whereas river basins along the southwestern and northeastern OBR generally have lower MLS values. The characteristics of knickpoints identified in our analysis are also shown. YD: Yakeishi Dake

To further test if the k_{sn} patterns are produced by differences of lithology, we analyzed k_{sn} values of river basins in two nearby regions west of the OBR, one to the north and the other to the south of the Yokote Basin, where the lithology is similar to the OBR but no active faults were identified (Fig. 6). In these two areas, rivers flow through four major types of bedrocks that are similar in age: sedimentary rocks with some tuff, volcanic rocks, volcanic rocks with some sedimentary rocks, and tuff. These rock types are also the major rock types found in the OBR (Figs. 3 and 6). In each of these two areas, the average k_{sn} values of river segments flowing through these different rock types vary, but overlap within uncertainties, showing no systematic variations caused by rock

Table 1 Basin-wide mean local steepness (MLS) data of the 31 river basins analyzed in this study, together with previously published vertical separation rates of the two fault systems in the corresponding areas

No	Area	Basin area (km^2)	Mean local steepness	Weighted average MLS	Published fault vertical rates (mm/yr)
1	NW	9.65578	60.67	60.66	0.4–1.3
2	NW	39.7108	70.05		
3	NW	17.4968	70.26		
4	NW	10.8431	58.64		
5	NW	10.9370	23.89		
6	NW	42.2993	57.89		
7	SW	6.75494	36.37	34.41	0.1–0.4
8	SW	7.42205	29.99		
9	SW	101.0420	31.67		
10	SW	87.5279	28.02		
11	SW	5.7846	19.04		
12	SW	257.6540	38.08		
13	NE	6.7463	41.49	34.40	0.2–0.6
14	NE	2.3849	36.34		
15	NE	50.1790	27.29		
16	NE	33.0572	36.40		
17	NE	19.6266	26.79		
18	NE	14.9837	27.32		
19	NE	101.2140	37.02		
20	NE	9.9853	34.97		
21	NE	5.3751	25.54		
022	NE	15.3485	35.60		
23	NE	31.9513	37.70		
24	NE	12.0159	42.73		
25	NE	77.6148	35.01		
26	SE	21.1544	55.58	48.31	0.4–0.5
27	SE	51.1843	51.87		
28	SE	9.2057	16.59		
29	SE	20.4161	36.22		
30	SE	34.5379	41.52		
31	SE	191.2260	50.60		

type differences (Fig. 6). Therefore, we conclude that the differences in rock types do not produce significant k_{sn} differences in the OBR rivers.

We propose that the k_{sn} patterns in OBR rivers are primarily produced by differences in the activities of the active faults along the OBR mountain fronts. The generally higher MLS values for the river basins along the northwestern OBR front indicate that rivers there have generally steeper valleys, whereas the generally lower MLS values for the southwestern OBR rivers indicate that they have gentler river valleys. Under similar climatic and lithological conditions, this would suggest that the northwestern OBR has higher uplift rates than the southwestern OBR.

The OBR is bounded on its two sides by the EFZYB and the WFZKL, both of which are primarily dip-slip reverse faults (Headquarters for Earthquake Research Promotion 2001, 2005a). Therefore, the uplift patterns of the OBR flanks are likely reflecting the variations of vertical separation rates of the two fault systems. The northern EFZYB, for example, would have a higher vertical separation rate than the southern EFZYB to produce a higher uplift rate for the northwestern OBR. The vertical separation rates of faults are related to their actual slip rates and their dip angles. Although there are not many data about the subsurface geometry of the two fault systems, all available information indicates that their subsurface geometries are similar. Both fault systems have gentle

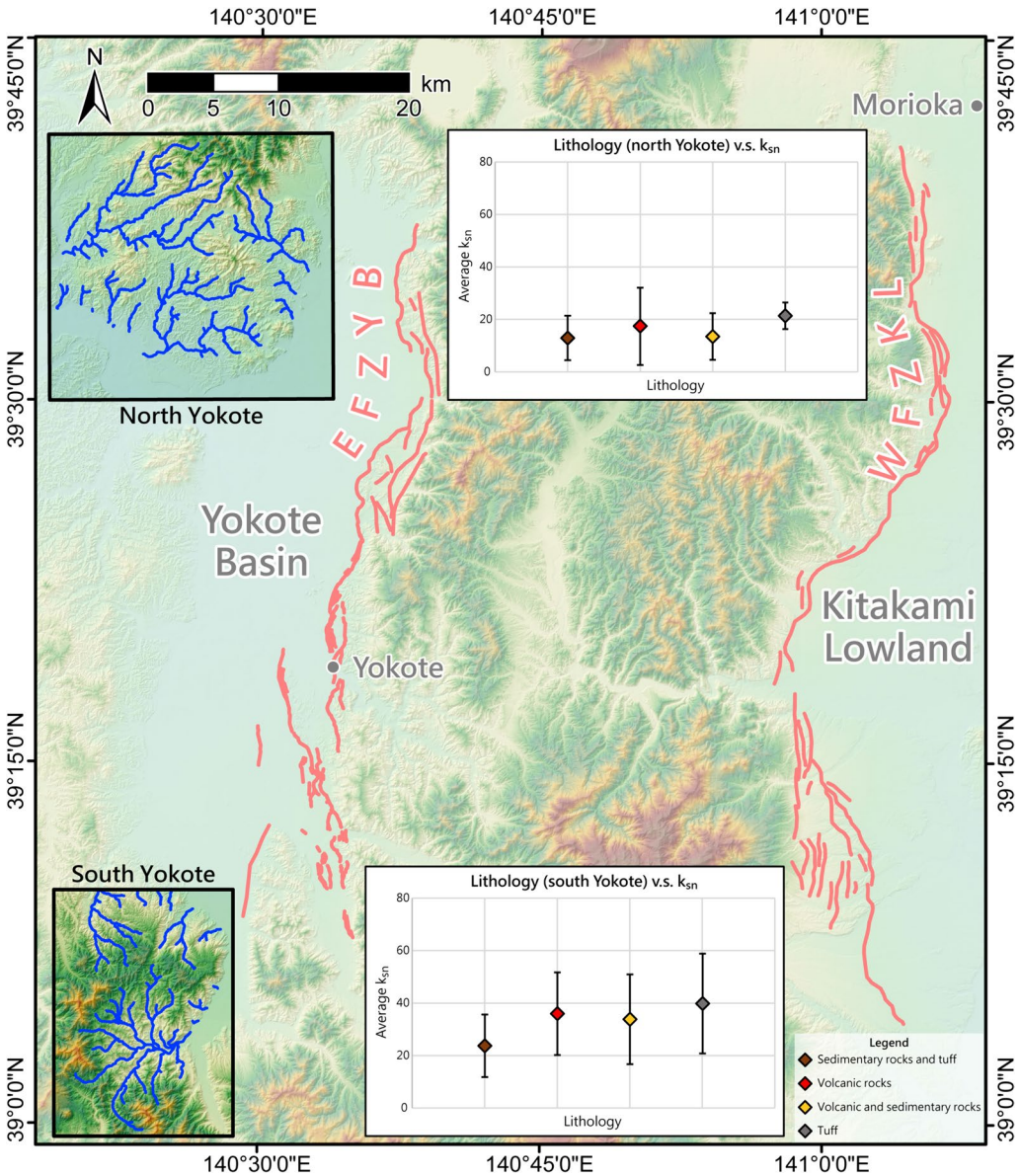

Fig. 6 Analysis of the relationship between lithology and channel steepness. We analyzed k_{sn} values of river basins in two nearby regions of the OBR, where the lithology is similar to the OBR but no active faults were identified, to test if the k_{sn} patterns are produced by differences of lithology. In each of these two areas, the average k_{sn} values of river segments flowing through different rock types overlap within each other's uncertainties, showing no systematic variations caused by rock type differences

dips of ~ 20°–35° at shallow depths, and become steeper at 30°–45° at deeper depths (Headquarters for Earthquake Research Promotion 2001; Sato et al. 2006; Kagohara et al. 2009, 2011; AIST 2010; Arora et al. 2021). There is also no apparent difference in the fault geometry from north to south. As a result, we propose that the MLS pattern illustrated in Fig. 5 is primarily produced by varying slip rates along different segments of the EFZYB and the WFZKL.

5.2 Structural activity patterns of the Ou Backbone Range

Based on the discussion above, we propose that the different MLS values shown in the river basins of OBR (Fig. 5) reflect different slip rates along the EFZYB and the WFZKL. We therefore divided both OBR fronts into northern and southern segments, and calculated the average MLS values (weighted with drainage basin areas) for the four mountain front segments. The northwestern OBR front has the highest average MLS value of 60.66,

albeit it also has a large scattering (Table 1). On the other hand, the southwestern and northeastern OBR fronts have significantly lower average MLS, and the average MLS value for the southeastern OBR front is somewhat in between.

Because the channel steepness is proportional to the uplift rate (e.g., Kirby and Whipple 2012), the nearly twice higher value of the average MLS along the northwestern OBR front than that along the southwestern OBR front suggests that the northwestern OBR is uplifting much faster than the southwestern OBR. Along the Shiraiwa fault and the Ota fault in the northern EFZYB, Mizumoto (2006) proposed a Holocene vertical separation rate of ~ 0.4–1.1 mm/yr based on the ages and offset amount of river terraces across the faults. Similarly, along the Senya fault in the northern EFZYB, Holocene and late Pleistocene vertical separation rates of ~ 0.9–1.3 mm/yr and ~ 0.8–0.9 mm/yr, respectively, have been proposed (Nakata 1976; Matsuda et al. 1980; Hirano 1984; Mizumoto 2006). Data points along the southern EFZYB are much fewer, but Akita Prefecture (1998a, b, 1999) found a much lower late Pleistocene to Holocene vertical separation rate across the fault of ~ 0.1–0.4 mm/yr. The patterns of these numbers are consistent with the variations of the average MLS values of the river basins. A similar uplift pattern is also reported by Tajikara and Ikeda (2005) using the height differences between fluvial terraces. As discussed above, the subsurface geometry of the EFZYB does not change significantly from north to south, and the slower uplift along the southern EFZYB likely represents lower slip rates of the fault. Therefore, based on our observations of river valley steepness, we suggest that the less constrained southern EFZYB does slip at a much lower rate than the northern segment.

On the eastern side, the southern segment of the eastern OBR front has higher average MLS than the northern segment. This pattern would suggest that the southeastern OBR is uplifting at a higher rate than the northeastern OBR, and the southern segment of the WFZKL slips at a higher rate than the northern segment. However, existing data do not show significant difference for uplift rates along the WFZKL (e.g., Tajikara and Ikeda 2005). For example, along the Nanshozan fault group, the Uwandaira fault group, and the Yokomoriyama fault in the northern WFZKL, Mizumoto (2006) calculated a Holocene vertical separation rate of ~ 0.3–0.5 mm/yr, and the late Pleistocene rate was suggested to be ~ 0.2–0.6 mm/yr (Watanabe 1991; Iwate Prefecture 1996, 1998a, b; Mizumoto 2006; Kagohara et al. 2011; Kosaka et al. 2013). These numbers are much lower than the rates along the northern EFZYB, consistent with the MLS patterns. Along the southern WFZKL, data points are also much fewer. Based on the ages of offset river terraces, Mizumoto (2006) calculated a Holocene vertical separation rate of ~ 0.5 mm/yr, and Iwate Prefecture (1998a, b) proposed a late Pleistocene rate of ~ 0.4 mm/yr. These numbers are all similar.

We suggest that the slightly higher average MLS values in southeastern OBR may have been produced by young pyroclastic materials in the vicinity of the Yakeishi Dake (Fig. 3). In our analysis, we have avoided the areas with Holocene active volcanoes to prevent the influences of volcanism on the uplift and incision of rivers. However, although the Yakeishi Dake is not active in the Holocene, its last activity at ca. 0.2 Ma had produced a large amount of pyroclastic materials (Nakano et al. 2013; Geological Survey of Japan, AIST 2020, 2023). These pyroclastic deposits may have filled up previous topography and rejuvenated river valleys in this area. Therefore, the presence of young pyroclastic materials from the Yakeishi Dake may have contributed to the steepening of river channels in the southeastern OBR.

5.3 Implications for future earthquake hazards

The OBR is one of the most prominent topographic features in the Tohoku Region of Japan. The two active fault systems bounding the two sides of the OBR are both major active fault systems in Japan, and pose important earthquake hazard potentials for the region. The northern segment of the EFZYB, for example, is the seismogenic structure of the 1896 M7.2 Rikuu earthquake, which had resulted in more than 200 casualties (Matsuda et al. 1980). Although there have been many studies on the activities of these two major active fault systems, information on segments other than the northern EFZYB is still limited. As a result, it is still unclear whether the southern segment of the EFZYB is as active as the northern segment and poses similar earthquake hazard potential.

Our geomorphic analysis results on river basins flowing out of both OBR fronts suggest that the northwestern OBR front has the steepest river valleys. This implies that the northern segment of the EFZYB has the highest slip rates among the different segments of the EFZYB and the WFZKL. This is consistent with the available slip rate data of the two fault systems, and the fact that the surface rupture during the 1896 Rikuu earthquake was limited in the northern segment of the EFZYB. If this is correct, the earthquake recurrence intervals for the other segments of the two fault systems would be longer than the ~ 3500 years proposed for the northern EFZYB (e.g., Imaizumi et al. 1989a, 1989b). For example, if we assume the slip rates of those segments are only about a half of the rate of northern EFZYB as implies by the MLS patterns, and the average slip per earthquake event is similar for all segments, the earthquake recurrence intervals for

those segments would be around 7000 years, and longer if the average slip per event is larger. This would be consistent with previous estimations (e.g., Headquarters for Earthquake Research Promotion 2001, 2005a).

However, since there are not many constraints for the timing of the last rupture event for those fault segments (e.g., Headquarters for Earthquake Research Promotion 2001, 2005a), a longer recurrence interval does not mean that the probability for an earthquake occurring in the near future is low. More detailed paleoseismological information on these two major fault systems is still needed for a better understanding of future earthquake hazard potentials for this region.

6 Conclusions

In this study, we analyzed the steepness indexes of 31 river basins that flow out of the two flanks of the OBR. Along the western OBR front, river basins in the north have steeper valleys than those in the south, and river basins along the northeastern OBR front have slightly gentler valleys than those along the southeastern OBR front. We have found knickpoints in these river basins, but most of them are related to local lithologic boundaries or are check dams. Therefore, we suggest that the river steepness patterns are reflecting variations in uplift rates along the OBR flanks, which in turn reflecting the structural activities of the EFZYB and the WFZKL, the two major active fault systems on both sides of the OBR.

Our results suggest that the northern segment of the EFZYB has a higher slip rate than the southern segment. This is consistent with results of previous studies and the fact that the 1896 M7.2 Rikuu earthquake only ruptured the northern segment of the EFZYB. Therefore, the earthquake recurrence intervals for the southern segment of the EFZYB or the WFZKL would be longer than the published ~ 3500 years for the northern EFZYB. However, since there is no good constraint for the last earthquake event along these segments, more paleoseismological studies on these two major fault systems is still needed.

Supplementary Information

The online version contains supplementary material available at https://doi.org/10.1186/s40645-024-00644-9.

Additional file 1

Additional file 2

Acknowledgements

We are grateful for the enlightening discussions with T. Imaizumi, T. Nakata, and Y. Ota. We would like to thank C.-H. Chen, S.-C. Liu, C.-H. Tsai and Y.-H. Yin for the assistance in the field investigations, and H.L.B. Chou for preparing the figures of this paper. We appreciate the comments and suggestions from N. Toke and an anonymous reviewer, which significantly improved this manuscript. This study was partly supported by the World Premier International Research Center Initiative (WPI), MEXT, Japan.

Author contributions

JBHS contributed to conceptualization, investigation, visualization, project administration, funding acquisition, writing-original draft preparation, and writing-review and editing. JHL contributed to formal analysis, investigation, visualization, and writing—original draft preparation. CYC contributed to methodology, software, investigation, and writing—review and editing. HT contributed to data curation and writing—review and editing. YI contributed to investigation and writing—review and editing. All authors have read and approved the final version of the manuscript.

Funding

This research was supported by the National Science and Technology Council (NSTC) of Taiwan (108-2116-M-002-016-MY2, 110-2116-M-002-019, and 111-2116-M-002-044 to JBHS).

Availability of data and materials

The 10-m resolution DEM of Japan analyzed in this study is available from the Geospatial Information Authority of Japan at https://www.gsi.go.jp/top.html. The geologic map of the study area is available from the Geological Survey of Japan at https://gbank.gsj.jp/seamless/v2/viewer/. The annual precipitation data are from https://nlftp.mlit.go.jp/ksj/gml/datalist/KsjTmplt-G02.html. The channel steepness index data generated in this study are included in Table 1.

Competing interests

The authors declare that they have no competing interests.

Received: 11 December 2023 Accepted: 28 June 2024
Published online: 10 July 2024

References

AIST (2010) Investigations on the Activities and the Rupture History of the Eastern Fault Zone of Yokote Basin (Southern Part), Report No. H21–2, Additional and Complementary Investigations on Active Faults, National Institute of Advanced Industrial Science and Technology, Tsukuba, p 77. (in Japanese) Retrieved from https://www.jishin.go.jp/main/chousakenkyuu/tsuika_hokan/h21_yokote.pdf

Akita Prefecture (1998) Report of Investigation Results on the Eastern Fault Zone of Yokote Basin. Grants for Fundamental Investigations for Earthquakes in 1997, p 103. (in Japanese) Retrieved from https://www.hp1039.jishin.go.jp/danso/Akita3frm.htm

Akita Prefecture (1999) Report of Investigation Results on the Eastern Fault Zone of Yokote Basin. Grants for Fundamental Investigations for Earthquakes in 1998, p 150. (in Japanese) Retrieved from https://www.hp1039.jishin.go.jp/danso/Akita3Bfrm.htm

Arora S, Kondo H, Kurosawa H, Koshika K (2021) Estimation of the slip rate along the unruptured fault segment of the M72 1896 Rikuu earthquake, northeast Japan. Tectonics 40:e2020TC006434. https://doi.org/10.1029/2020TC006434

Chen C-Y, Willett SD (2016) Graphical methods of river profile analysis to unravel drainage area change, uplift and erodibility contrasts in the Central Range of Taiwan. Earth Surf Proc Landforms 41:2223–2238. https://doi.org/10.1002/esp.3986

Chen C-Y, Willett SD, Christl M, Shyu JBH (2021) Drainage basin dynamics during the transition from early to mature orogeny in Southern Taiwan. Earth Planet Sci Lett 562:116874. https://doi.org/10.1016/j.epsl.2021.116874

Chen Y-W, Shyu JBH, Chang C-P (2015) Neotectonic characteristics along the eastern flank of the Central Range in the active Taiwan orogen inferred from fluvial channel morphology. Tectonics 34:2249–2270

Cyr AJ, Granger DE, Olivetti V, Molin P (2010) Quantifying rock uplift rates using channel steepness and cosmogenic nuclide-determined erosion rates: examples from northern and southern Italy. Lithosphere 2:188–198

DiBiase RA, Whipple KX, Heimsath AM, Ouimet WB (2010) Landscape form and millennial erosion rates in the San Gabriel Mountains, CA. Earth Planet Sci Lett 289:134–144. https://doi.org/10.1016/j.epsl.2009.10.036

DeLisle C, Yanites B, Chen C-Y, Rittenour T, Shyu JBH (2022) Extreme event driven sediment aggradation and erosional buffering along a tectonic gradient in southern Taiwan. Geology 50:16–20

Geological Survey of Japan, AIST (ed.) (2020) Geologic Map of Volcanoes in Japan (1:200,000), version 1.0d. Geological Survey of Japan, AIST. (https://gbank.gsj.jp/volcano/vmap/)

Geological Survey of Japan, AIST (2023) Seamless digital geological map of Japan V2 (1:200,000), Original edition. (https://gbank.gsj.jp/seamless/)

Goto N, Sasaki T (2019) Estimation of activity of a blind fault using the spatial variation of the relative heights of fluvial terraces: an example of the Iwai river above the focal area of the 2008 Iwate-Miyagi Nairiku earthquake. Quat Res 58:315–331 (**in Japanese with English abstract**)

Harkins N, Kirby E, Heimsath A, Robinson R, Reiser U (2007) Transient fluvial incision in the headwaters of the Yellow River, northeastern Tibet, China. J Geophys Res Earth Surf 112:F03S04

Harvey JE, Burbank DW, Bookhagen B (2015) Along-strike changes in Himalayan thrust geometry: Topographic and tectonic discontinuities in western Nepal. Lithosphere 7:511–518

Headquarters for Earthquake Research Promotion (2001) Evaluation of the Western Fault Zone of Kitakami Lowland, p 25. (in Japanese) Retrieved from https://www.jishin.go.jp/main/chousa/katsudansou_pdf/13_kitakami-teichi.pdf

Headquarters for Earthquake Research Promotion (2005a) Long-term Evaluation of the Eastern Fault Zone of Yokote Basin, p 23. (in Japanese) Retrieved from https://www.jishin.go.jp/main/chousa/katsudansou_pdf/15_yokote-bonchi.pdf

Headquarters for Earthquake Research Promotion (2005b) Long-term Evaluation of the Western Fault Zone of Shizukuishi Basin and the Eastern Fault Zone of Mahiru Mountains, p 26. (in Japanese) Retrieved from https://www.jishin.go.jp/main/chousa/katsudansou_pdf/14_shizukuishi_mahiru.pdf

Headquarters for Earthquake Research Promotion (2009) Seismic Activities of Japan, Regional Characteristics from the Perspective of Damaging Earthquakes, 2nd Version, 496 pp. (in Japanese) Retrieved from https://www.jishin.go.jp/resource/seismicity_japan/

Hirano S (1984) Estimation of the period of prehistoric large earthquake occurrence along the Senya Fault System in Tohoku district, northeast Japan. Geogr Rev Japan Ser A 57:173–185 (**in Japanese with English abstract**)

Howard AD, Kerby G (1983) Channel changes in badlands. Geol Soc Am Bull 94:739–752

Imaizumi T, Miyauchi T, Yoshioka T, Suzuki T, Matsuda T, Suzuki Y, Hayakawa T, Sakurai K, Kashiwagi S, Togo M, Yamaguchi S, Fukasawa H, Osugi Y, Kumasawa H (1989a) Trench investigations of the Senya fault (Hanaoka area) in 1985. Active Fault Res 6:81–86 (**in Japanese**)

Imaizumi T, Miyauchi T, Suzuki T, Yamagata K, Hirano S, Matsuda T (1989b) Trench investigations of the Senya fault (Ichijogi south area) in 1988. Active Fault Res 6:87–92 (**in Japanese**)

Imaizumi T, Sato H, Ikeda Y, Ishimaru K, Sakai R, Yoneda S, Kubota H (1997) Near-surface feature and slip-rate of the Senya fault, Akita Prefecture, detected by drilling. Progr Abstr Jpn Assoc Quat Res 27:84–85 (**in Japanese**)

Iwate Prefecture (1996) Report of Investigation Results on the Western Fault Zone of Shizukuishi Basin, Hanamaki Fault Zone, and Kitakami West Fault Zone. Grants for Fundamental Investigations for Earthquakes in 1995, p 174. (in Japanese) Retrieved from https://www.hp1039.jishin.go.jp/danso/Iwate3Afrm.htm

Iwate Prefecture (1997) Report of Investigation Results on the Western Fault Zone of Kitakami Lowland. Grants for Fundamental Investigations for Earthquakes in 1996, 74 pp. (in Japanese) Retrieved from https://www.hp1039.jishin.go.jp/danso/Iwate3Bfrm.htm

Iwate Prefecture (1998) Report of Investigation Results on the Western Fault Zone of Kitakami Lowland. Grants for Fundamental Investigations for Earthquakes in 1997, p 60. (in Japanese) Retrieved from https://www.hp1039.jishin.go.jp/danso/Iwate4frm.htm

Kagohara K, Ishiyama T, Imaizumi T, Miyauchi T, Sato H, Matsuta N, Miwa A, Ikawa T (2009) Subsurface geometry and structural evolution of the eastern margin fault zone of the Yokote basin based on seismic reflection data, northeast Japan. Tectonophysics 470:319–328. https://doi.org/10.1016/j.tecto.2009.02.007

Kagohara K, Kosaka H, Miwa A, Imaizumi T, Mamada Y (2011) Active tectonics along the western margin of Kitakami Lowland: tectonic geomorphology and subsurface structure of the Nanshozan Fault Group, northeast Japan. J Geogr 120:910–925 (**in Japanese with English abstract**)

Kirby E, Ouimet W (2011) Tectonic geomorphology along the eastern margin of Tibet: insights into the pattern and processes of active deformation adjacent to the Sichuan Basin. In: Gloaguen R, Ratschbacher L (eds) Growth and Collapse of the Tibetan Plateau. Geological Society, London, pp 165–188

Kirby E, Whipple KX (2012) Expression of active tectonics in erosional landscapes. J Struct Geol 44:54–75. https://doi.org/10.1016/j.jsg.2012.07.009

Kosaka H, Kagohara K, Imaizumi T, Miwa A, Abe K (2013) Fault topography and fault outcrop around the southern end of the Uwandaira Fault Group in the Kitakami Lowland Western Marginal Fault Zone, northeast Japan. Geogr Rev Jpn Ser A 86:493–504 (**in Japanese with English abstract**)

Matsuda T, Yamazaki H, Nakata T, Imaizumi T (1980) The surface faults associated with the Rikuu earthquake of 1896. Bull Earthq Res Inst Univ Tokyo 55:795–849 (**in Japanese with English abstract**)

Matsu'ura T, Kase Y (2010) Late Quaternary and coseismic crustal deformation across the focal area of the 2008 Iwate-Miyagi Nairiku earthquake. Tectonophysics 487:13–21

Matsu'ura T, Sugaya K (2017) Late Quaternary crustal shortening rates across thrust systems beneath the Ou Ranges in the NE Japan arc inferred from fluvial terrace deformation. J Asian Earth Sci 140:13–30

Matsu'ura T, Furusawa A, Saomoto H (2008) Late Quaternary uplift rate of the northeastern Japan arc inferred from fluvial terraces. Geomorphology 95:384–397

Miller SR, Sak PB, Kirby E, Bierman P (2013) Neogene rejuvenation of central Appalachian topography: evidence for differential rock uplift from stream profiles and erosion rates. Earth Planet Sci Lett 369–370:1–12

Mizumoto T (2006) Geomorphic evidence of paleoearthquakes during Holocene on principal thrust fault zones in the Tohoku district, northeast Japan. Sci Rep Tohoku Univ, Ser 7 (Geography) 55:1–69.

Nakano S, Nishiki K, Takarada S, Hoshizumi H, Ishizuka Y, Itoh J, Kawanabe Y, Oikawa T, Furukawa R, Geshi N, Ishizuka O, Yamamoto T, Kisimoto K (2013) Volcanoes in Japan (3rd Version), Geological Survey of Japan, AIST, 1:2,000,000 Geological Map Series, no. 11.

Nakata T (1976) Quaternary tectonic movements in central Tohoku district, northeast Japan. Sci Rep Tohoku Univ, Ser 7 (Geography) 26:213–239.

Nakata T, Imaizumi T (2002) Digital active fault map of Japan. University of Tokyo Press, Tokyo, p 60

Ogami T (2015) Dynamics of longitudinal river profiles associated with knickpoints since the Middle Pleistocene on the northern Sanriku Coast, NE Japan. Quat Res 54:113–128 (**in Japanese with English abstract**)

Perron JT, Royden L (2012) An integral approach to bedrock river profile analysis. Earth Surf Proc Landforms 38:570–576. https://doi.org/10.1002/esp.3302

Regalla C, Kirby E, Fisher D, Bierman P (2013) Active forearc shortening in Tohoku, Japan: constraints on fault geometry from erosion rates and fluvial longitudinal profiles. Geomorphology 195:84–98

Research Group for Active Faults of Japan (Eds.) (1991) Active Faults in Japan: Sheet Maps and Inventories. University of Tokyo Press, Tokyo, p 437 (Revised Edition)

Research Group for the Senya Fault (1986) Holocene activities and near-surface features of the Senya Fault, Akita Prefecture, Japan—Excavation study at Komori, Senhata-cho. Bull Earthq Res Inst Univ Tokyo 61:339–402 (**in Japanese with English abstract**)

Sawa S, Tsutsumi H, Sugito N, Kagohara K (2013) Explanatory text for "Lake Tazawa," "Yokote," and "Yuzawa," 1:25,000 Active Fault Map in Urban Area: The Eastern Boundary Fault Zone of the Yokote Basin and its vicinity. Geospatial Information Authority of Japan Technical Data D1-No.642, pp 24. (in Japanese)

Sato H, Hirata N, Iwasaki T, Matsubara M, Ikawa T (2002) Deep seismic reflection profiling across the Ou Backbone range, northern Honshu Island, Japan. Tectonophysics 355:41–52

Sato H, Ikeda Y, Imaizumi T, Mikada H, Toda S, Tsutsumi H, Koshiya S, Noda K, Ito T, Miyauchi T, Yagi H, Togo M, Iwasaki T, Saka M, Hirata N, Matsuta N, Kawamura T, Ishimaru K, Ikawa T, Senya 96 Seismic profiling group (2006) High-resolution seismic reflection profiling across the Senya fault at Hanaoka, northern Honshu, Japan: data acquisition and processing.

Bull Earthq Res Inst Univ Tokyo 81:97–106 (**in Japanese with English abstract**)
Schwanghart W, Scherler D (2014) Short communication: TopoToolbox 2—MATLAB-based software for topographic analysis and modeling in Earth surface sciences. Earth Surf Dyn 2:1–7. https://doi.org/10.5194/esurf-2-1-2014
Tajikara M, Ikeda Y (2005) Vertical crustal movement and development of basin and range topography in the middle part of the northeast Japan arc estimated from fluvial/marine terrace data. Quat Res 44:229–245 (**in Japanese with English abstract**)
Tajikara M, Ikeda Y, Nohara T (2009) Surface fault of the Iwate-Miyagi Nairiku earthquake in 2008 estimated by distribution of heights of fluvial terraces. Zisin 62:1–11 (**in Japanese with English abstract**)
Takahashi N, Shyu JBH, Chen C-Y, Toda S (2022) Long-term uplift pattern recorded by rivers across contrasting lithology: insights into earthquake recurrence in the epicentral area of the 2016 Kumamoto earthquake. Jpn Geomorphol 419:108492. https://doi.org/10.1016/j.geomorph.2022
Takahashi NO, Shyu JBH, Toda S, Matsushi Y, Ohta RJ, Matsuzaki H (2023) Transient response and adjustment timescales of channel width and angle of valley-side slopes to accelerated incision. J Geophys Res Earth Surf 128:e2022JF006967. https://doi.org/10.1029/2022JF006967
Toda S, Maruyama T, Yoshimi M, Kaneda H, Awata Y, Yoshioka T, Ando R (2010) Surface rupture associated with the 2008 Iwate-Miyagi Nairiku, Japan, earthquake and its implications to the rupture process and evaluation of active faults. Zisin 62:153–178 (**in Japanese with English abstract**)
Watanabe M (1989) Complementary distributions of active faults and Quaternary volcanoes, and tectonic movements, along the volcanic front of northeast Japan. Bull Dep Geogr Univ Tokyo 21:37–74
Watanabe M (1991) Chronology of the fluvial terrace surfaces in the Kitakami Lowland, northeast Japan, and fluctuations of debris supply during the Late Pleistocene. Quat Res 30:19–42 (**in Japanese with English abstract**)
Watanabe M, Ikeda Y, Suzuki Y, Sugai T (1994) Paleoseismicity and fault structure of the Western Boundary Active Faults of the Kitakami Lowland, northeast Japan: excavation study of the Uwandaira Fault Group, west of Hanamaki City. Geogr Rev Jpn Ser A 67:393–403 (**in Japanese with English abstract**)
Whipple KX, Tucker GE (1999) Dynamics of the stream-power river incision model: implications for height limits of mountain ranges, landscape response timescales, and research needs. J Geophys Res: Earth Surf 104:17661–17674. https://doi.org/10.1029/1999jb900120

Publisher's Note